Article

Electrospun Poly (vinylidene fluoride-co-hexafluoropropylene) nanofibers membranes for brine treatment by membrane distillation

Amjad Albiladi [1,2], Lassaad Gzara [1], Hussam Organji [1] and Nazeeha Alkyal [2]. Alberto Figoli[3]

[1] Center of Excellence in Desalination Technology, King Abdulaziz University, P.O. Box: 80200, Jeddah 21589, Saudi Arabia.; lgzara@kau.edu.sa

[2] Chemistry Department, Faculty of Science, King Abdulaziz University, Jeddah, Saudi Arabia.

[3] Institute on Membrane Technology (ITM-CNR), Via P. Bucci 17c, 87036 Rende, CS, Italy

Abstract: The major challenge for membrane distillation (MD) is membrane wetting resistance induced by pollutants in the feed solution. The proposed solution for this issue was to fabricate membranes with hydrophobic properties. Hydrophobic electrospun Poly (vinylidene fluoride-co-hexafluoropropylene) (PVDF-HFP) nanofibers membranes were produced for brine treatment using the direct contact membrane distillation (DCMD) technique. These nanofibers membranes were prepared from three different polymeric solution compositions to study the effect of solvent composition in the electrospinning process. Further, the effect of the polymer concentration was investigated by preparing polymeric solutions with three different polymer percentages: 6, 8, and 10%. All nanofibers membranes obtained from electrospinning were post-treated at varying temperatures. The effects of thickness, porosity, pore size, and LEP were studied. The hydrophobicity was determined by contact angle measurements, which were investigated by optical contact angle goniometry. The crystallinity and thermal properties were studied by DCS and XRD, while the functional groups were studied by FTIR. The morphological study was performed by AMF and described the roughness of nanofibers membranes. Finally, all nanofibers membranes have enough of a hydrophobic nature to be used in DCMD. PVDF membrane filter disc and all nanofibers membranes were applied in DCMD to treat brine water. The resulting water flux and permeate water quality were compared, and it was discovered that all produced nanofibers membranes showed good behavior with varying water flux, but the salt rejection was greater than 90%. A membrane prepared from DMF/acetone 5-5 with 10% PVDF-HFP provided perfect performance, with an average water flux of 44 $kg.m^{-2}.h^{-1}$ and salt rejection of 99.8%.

Keywords: polyvinylidene fluoride-co-hexafluoropropylene (PVDF-HFP); Electrospinning; Nanofibers; Hydrophobic membrane; Membrane distillation

1. Introduction

Throughout the ages, water scarcity has remained the biggest problem in the world that is faced by many countries, which is still one of the most important global challenges to date. Despite 70% of the Earth's being water, only less than 3% of that is pure water, and it is unequally distributed around the world. However, the natural underground water is threatened with depletion due to increased demand without control [1–3]. To address this rapidly growing issue, a group of scientists has begun to look into the production of freshwater using a variety of low-cost and environmentally friendly technologies [4,5]. Researchers have focused on seawater desalination and wastewater treatment to alleviate the demand for freshwater, and these two sources are largely abundant. For a long time, water desalination operations have consumed a lot of energy which indicates that they were very costly processes [6,7]. Membrane separation technologies have been extensively researched in recent years due to their unique characteristics such as high quality of treated water and low operational and energy costs [8]. Membrane-based technologies are classified into microfiltration (MF),

ultrafiltration (UF), nanofiltration (NF), reverse osmosis (RO), forward osmosis (FO), and membrane distillation (MD) depending on the diameter of pores and membrane separation properties. Furthermore, the main difference between all previous membrane-based techniques and MD is that the MD is a thermally driven process while the others are pressure-driven operations [8]. Among all these membrane-based techniques, the membrane distillation (MD) technique has received great attention due to its various advantages compared to other techniques, including (i) high salt rejection (>99.9%), (ii) significantly larger pore size, (iii) lower fouling sensitivity, (iv) reduced feed salinity sensitivity, (v) ability to use low-grade heat (40-80 °C), (vi) renewable energy can be used to heat the feed solution, which can be generated by waste heat from co-generation plants, and solar energy [9–11]. The Membrane Distillation (MD) process is based on the difference in vapor pressure between feed and permeation solutions created by the temperature gradient [12]. A large number of studies have preferred the use of polymeric membranes due to their low cost, high separation selectivity, and good separation performance. The typical examples of polymers utilized in MD research are polyvinylidene fluoride (PVDF), Polyethersulfone (PES), polyethylene (PE), polypropylene (PP), polyvinyl alcohol (PVA), polystyrene (PS), and polytetrafluoroethylene (PTFE). PVDF is a semi-crystalline fluorocarbon homo-polymer that possesses special properties such as excellent chemical resistance, hydrophobicity, and thermal and mechanical properties. In addition, due to PVDF having good solubility in some common polar organic solvents, it is easy to handle [1,13,14]. All these properties make PVDF an excellent candidate for membrane fabrication that is utilized for different purposes such as water purification [15,16], Lithium-ion batteries [17–19], gas separation [20], etc. PVDF polymer is categorized as piezoelectric material. The crystalline polymorphs of PVDF are formed depending on the various processing methods. There are five crystalline polymorphs of PVDF, which are α, β, γ, δ, and ε phases. The common three phases are the main phases of PVDF that were explained in Fig. 1 Those five crystal structures were divided into polar and non-polar phases. Polar phases include β and γ-phases, which determine the ferroelectric and piezoelectric properties of PVDF. Among these structures, the β-phase has a higher polarity than the others (γ and δ phases), but they also have polar unit cells. The piezoelectricity property of the β-phase is better than that of the γ-phase because of the presence of a gauche bond, which appears in every fourth repeat unit [21–24].

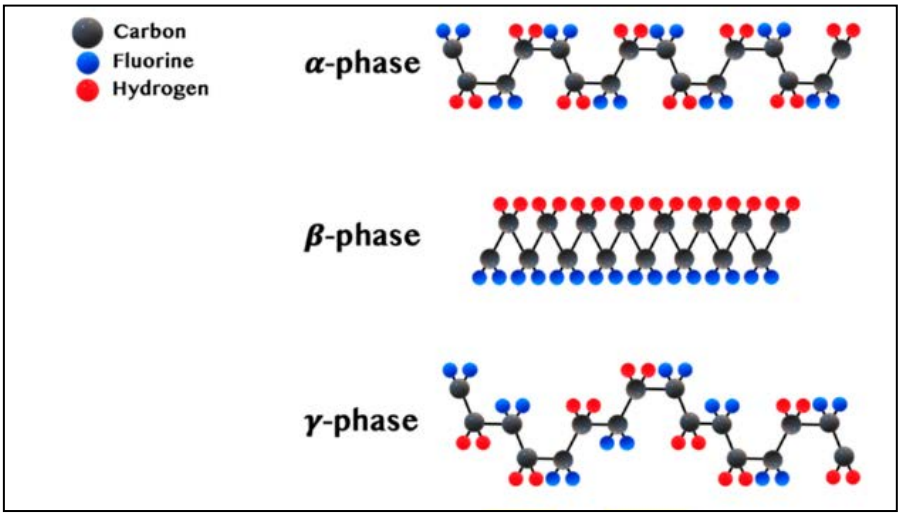

Fig.1 The essential phases of PVDF [22].

Poly (vinylidene fluoride-co-hexafluoropropylene) (PVDF-HFP) is a co-polymer resulting from vinylidene fluoride (VDF) and hexafluoropropylene (HFP) when they underwent emulsion polymerization. The incorporation of the HFP group in VDF polymer is responsible for improving its properties because the fluorine segment has a high hydrophobicity and lower polarity. Thus, PVDF-HFP possesses higher solubility (especially in organic solvents), higher hydrophobicity, better mechanical strength, lower glass transition temperature, lower crystallinity, and higher free volume compared with PVDF [25,26].

PVDF-HFP nanofibers membranes have been produced by several techniques for different applications but among those methods, electrospinning has proven to be effective in producing membranes with high efficiency and better properties. Briefly, it is making the preferred phase of PVDF (β-phase) which enhances voltage when the mechanical stress, strain, and bending activities were applied. During the fabrication of nanofibers, it can be produced and enhanced piezoelectricity properties in films due to polymer jet elongation. Hence, high-performance polymer films are usually produced by electrospinning which involves a high electric field applied to the polymer [22].

Electrospinning is a promising simple method for fabricating nano-fiber membranes for an extended variety of applications. As shown in Fig.2, it has three main parts: (i) a high-voltage supply. (ii) a spinneret with the polymer solution, (iii) and a grounded collector. When a high voltage is applied, the fine fibers will be produced from the polymer solution, where the polymer jet comes through the needle of the syringe and spins until collected in the collector as fibers in the form of a few nanometers to micrometers [8,27].

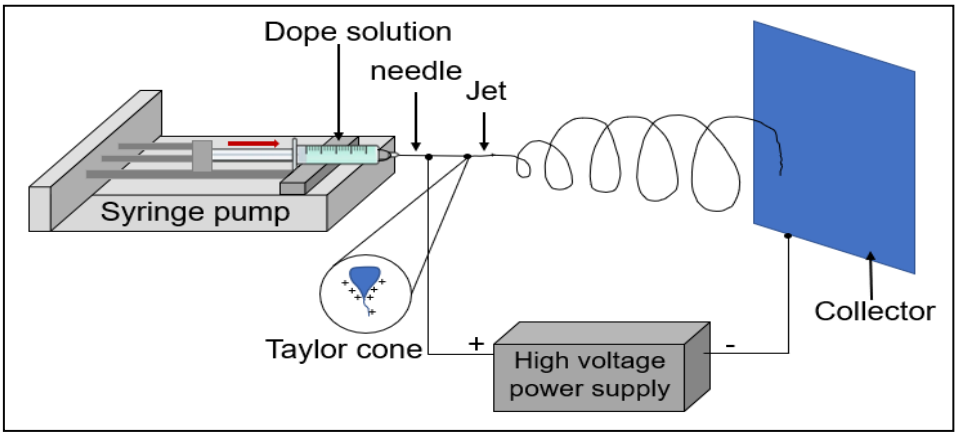

Fig.2 Electrospinning process and its components

The desired membrane structure can be controlled by tuning its preparation conditions, including the chemical structure of polymeric solutions and operational and environmental parameters. The morphology of the membrane depends on solvents since they influence the kinetic and thermodynamic parameters of solvent-polymer interaction.

The efficiency of desalination techniques that operate with membranes depends on the membrane's properties. Salt rejection and water flux are the basic properties that must be considered during the desalination process. In fact, flux and salt rejection are affected by porosity, pore size, and the high specific surface area of the electrospun nanofibers membrane. The better MD membrane usually has high liquid entry pressure (LEP), low thermal conductivity, low fouling rate, excellent chemical and thermal stability, and excellent mechanical strength. In the last few years, the membrane has been improved until the membrane-based desalination techniques have become operational with minimum energy [1,28,29]. There are different types of MD operation, namely, direct contact membrane distillation (DCMD), vacuum membrane distillation (VDM), air gap membrane distillation (AGMD), and sweeping gas membrane distillation (SGMD).

Direct contact membrane distillation (DCMD) is the simplest form of the MD, where both sides of feed and permeate are in direct contact through the process. This procedure is driven by a difference in temperature between the feed side and permeate side which leads to a difference in vapor pressure between them which drives the flux across the membrane [1,9]. The salt rejection factor of the PVDF-HFP copolymer nanofibers membrane was found to be higher than that of the PVDF homopolymer nanofibers membrane when they were employed in DCMD [30]. The electrospun PVDF nanofibers membrane was tested to treat a 3.5 wt% NaCl solution by DCMD, and the water permeation flux was about 21 kg m^{-2} h^{-1} [31].

This work aims to fabricate PVDF-HFP nanofibers membranes using the electrospinning technique for membrane distillation applications. In this work, Dimethylformamide (DMF)/Acetone mixture was chosen as a solvent to prepare the polymeric solutions. The effect of DMF/Acetone

 doi:10.20944/preprints202305.1577.v1

mixture composition and the polymer solution concentration on the morphology, crystallinity, and hydrophobicity of the developed electrospun PVDF-HFP nanofibers was assessed. Besides, the performance, in terms of flux and salt rejection, of the nanofibers membranes was assessed by the direct contact membrane distillation system (DCMD).

1. Experimental

2.1. Materials

Poly (vinylidene fluoride-co-hexafluoropropylene) PVDF-HFP Solef®21216 (Solvay Specialty Polymers, Bollate, Italy; Mw: 600,000 $g.mol^{-1}$) was dried for a few minutes at nearly 60 °C before use to remove any moisture. Acetone and N, N-Dimethylformamide (DMF) were used as solvents in different composition ratios, whereas lithium chloride (LiCl, anhydrous, 99%) was used as an additive. Except for PVDF-HFP, all chemicals were purchased from Sigma-Aldrich Company and used without further purification, Dope solutions preparation

PVDF-HFP dope solutions were prepared for electrospinning by dissolving a specific percentage of PVDF-HFP polymer in 50g of DMF and acetone solutions prepared with various weight ratios (6:4, 5:5, and 4:6 wt%). A suitable amount of LiCl (0.1%) was added to all dope solutions to develop dope electro-spin ability. Table 1. shows the preparation parameters of all dope solutions which were stirred for varying periods from an hour to one day at 60 °C until the polymer wholly dissolved. The homogenous dope solutions were degassed at room temperature overnight before electrospinning.

Table 1. Preparation parameters of each dope solution.

Dope solution abbreviation	Weight ratio (wt%) of solvents		PVDF-HFP %	LiCl %
	DMF	Acetone		
FA 6-4 P6	6	4	6	0.1
FA 6-4 P8	6	4	8	0.1
FA 6-4 P10	6	4	10	0.1
FA 5-5 P10	5	5	10	0.1
FA 4-6 P10	4	6	10	0.1

2.1. Membrane fabrication

All dope solutions underwent electrospinning to produce nanofibers membranes. Moreover, the efficiency of methods used to fabricate a hydrophobic membrane with desired properties, such as high porosity, narrow pores, and long-term performance, has been tested by fabricating membranes from one dope solution (FA 4-6 P10) by two methods, namely, electrospinning and the non-solvent induced phase separation (NIPS) method.

2.1.1. Electrospinning PVDF-HFP dope solutions

All membranes were carried out using a high-voltage power supply (22 kV) with a fixed needle tip (0.7 mm), and the distance between the needle and collector was 17 cm. Furthermore, the dope solution volume was 10 ml, and the flow rate was 1 ml/h for all polymeric solutions except FA 6-4 P8 and FA 6-4 P10 polymeric solutions, whose flow rates were reduced to 0.5 and 0.8 ml/h, respectively. Heat treatment has been applied to all electrospun membranes.

Post-heat treatment for all electrospun membranes has occurred to remove the residual solvent by putting them in the oven at 50 °C for an hour. Then the nanofibers membranes were put between two glass plates and left in the oven at 100 °C for a day. After that, further heat treatment was applied, which started at 140 °C for an hour under pressure, then the pressure was removed and the temperature was reduced by 10 °C per hour until it reached 100 °C, then left in the oven for a day.

2.1.1. The non-solvent induced phase separation (NIPS) method.

To make a comparison between electrospinning and NIPS methods that are used to fabricate hydrophobic membranes, the dope solution FA 4-6 P10 was used for electrospinning, as previously mentioned, whereas during the NIPS method, the same dope solution underwent a casting process at room temperature using a glass plate and a casting blade. Then it was kept for an hour before the coagulation bath to allow the solvents to evaporate. A coagulation water bath was applied to enable solvent and non-solvent exchange in the membrane matrix.

2.1. Characterizations of PVDF-HFP nanofibers membranes

The chemical and physical properties of electrospun nanofibers membranes were characterized using different techniques and mathematical relations.

2.1.1. Thickness, mean pore size, and LEP

The membrane thickness was measured in five different locations for all membranes using a digital micrometer and the average of those values was taken. The mean pore size (r_m) was calculated according to Guerout Elford Ferry's equation [55]:

$$r_m = \sqrt{\frac{(2.9 - 1.75\varepsilon)(8\eta l Q)}{\varepsilon A \Delta P}}$$

where η is the viscosity of water which is equal to 8.9×10^{-4} Pa s, ε and l are the porosity (%) and the thickness (μm) of the membrane, respectively, ΔP is the operation pressure (Pa), Q is the volume of permeate water per unit of time (m^3s^{-1}), and A is an effective area of the membrane (m^2) [15].

Liquid entry pressure (LEP) was measured for all membranes using a cylindrical pressure filtration cell with an effective surface area of 25.12 cm^2. The PVDF-HFP membrane was put on the bottom surface of the filtration cell, then it was pressed with 100 mL of distilled water and air, which were used as feed. The pressure began at 0.1 bar and was increased every 5 minutes or 30 seconds, depending on water flux, until it reached 2.5 bar. Then, the pressure was decreased by 1 bar every 5 minutes or 30 seconds until it reached the starting pressure. In both forward and backward directions, before increasing pressure, the mass of passed water was taken manually. LEP is defined as the pressure at which the first drop of water passes through the membrane and appears on the permeate side [32].

2.1.1. Porosity and water uptake

Firstly, the porosities and water uptake of PVDF-HFP nanofibers membranes were specified by immersion of 1 cm^2 of each membrane in pure water and kerosene separately for 24 h at room temperature. The wet weight was measured after wiping the excess amount of water or kerosene from the membranes' surface. Whereas the dried weight was obtained after drying membrane pieces in an oven at 50 ^{0}C overnight. Then the porosity (P%) and water uptake (WU%) were calculated based on the following equations:

$$P\% = \frac{\frac{W_w - W_d}{\rho_s}}{\frac{W_w - W_d}{\rho_s} + W_d/\rho_p} \times 100$$

$$WU\% = \frac{W_w - W_d}{W_d} \times 100$$

Where W_w and W_d are the wet and dried weights of the membrane (g), respectively, ϱ_s is the density of solvent (kerosene) used to stock membranes (g cm^{-3}), and ϱ_p is the density of polymer (PVDF). In porosity calculations, the wet and dried weights of membranes were taken with kerosene,

 doi:10.20944/preprints202305.1577.v1

but in water uptake measurements, the wet and dry weights of membranes were taken with distilled water [15,33].

2.1.1. Contact angle (CA)

For the evaluation of the membrane surface hydrophobicity, the water contact angle was measured for each membrane by an optical tensiometer instrument (Theta). In all measurements, distilled water was used. To reduce the experimental mistakes, the contact angles were measured for all membranes in three locations and the average number was reported.

2.1.1. DSC, FTIR, and XRD

Differential scanning calorimetry (DSC, 131 Evo) was used to determine the thermal properties and the crystal structure variation of the PVDF-HFP fibrous on all membranes at a heating and cooling rate of 5 K/min within the temperature range of 298–523 K.

Surface chemical compositions and functional groups of all membranes were analyzed using Cary 360 Fourier-transform infrared spectroscopy (FTIR) and all FTIR spectra were recorded by the attenuated total reflection (ATR) technique in the wavelength range of 4000- 400 cm^{-1}.

X-ray diffraction (XRD) patterns were studied using a Bruker D8 Advance with Cu Kα radiation (wavelength 1.5418 Å) at 40 kV and 40 mA. The patterns were collected between 2θ of 10° and 80°, and the scan speed was 1.5 degree/min.

2.1.1. Morphological studies: AFM

Atomic force microscopy (AFM) was used to study the morphological structure of the PVDF-HFP electrospun nanofibers membranes. The roughness and surface morphology of the PVDF-HFP membranes were analyzed by AFM. A small piece of each membrane was put on a glass substrate to be inserted into the AFM device. The AFM took an image of the membrane surface at a size of 10 μm×10 μm using the Gwyddion program which exhibits the roughness as peaks and valleys above the surface. The surface roughness can be studied in different terms like mean roughness (R_a), the root mean square of the Z data (R_q), and the mean difference between the five highest peaks and lowest valleys (R_z). However, the average roughness is the commonly utilized parameter for evaluating the surface roughness where its values are usually obtained by the Nanosurf CoreAFM software [34,35].

2.1.1. Membrane performance: DCMD tests Membrane

DCMD has been used for evaluating the electrospun PVDF-HFP membrane performance during the membrane distillation process. The DCMD setup is shown in Fig.3, where it contains two pumps, a feed/permeate tank, a digital balance, a flow meter, a conductivity meter, a heater, and a condenser. The feed tank was filled with real brine solution brought from a local seawater reverse osmosis (SWRO) plant. The feed side temperature was 70 ± 3 °C and the conductivity was 72 mS/cm. The permeate tank was filled with 1.5 L of distilled water with a conductivity below 2 µS/cm and then placed over the balance. The temperature of permeate side was kept constant at 20 ± 3 °C. The experiments were conducted at a constant pressure of 0.45 bar on both permeate and feed sides and the flow rate was 3 L/min. The steam of water passed from the hot feed side through the pores of the membrane to the permeate side.

The mass of transported water was recorded manually every 5 minutes for 2 hours. Then the flux of water (kg m^{-2} h^{-1}) was calculated as:

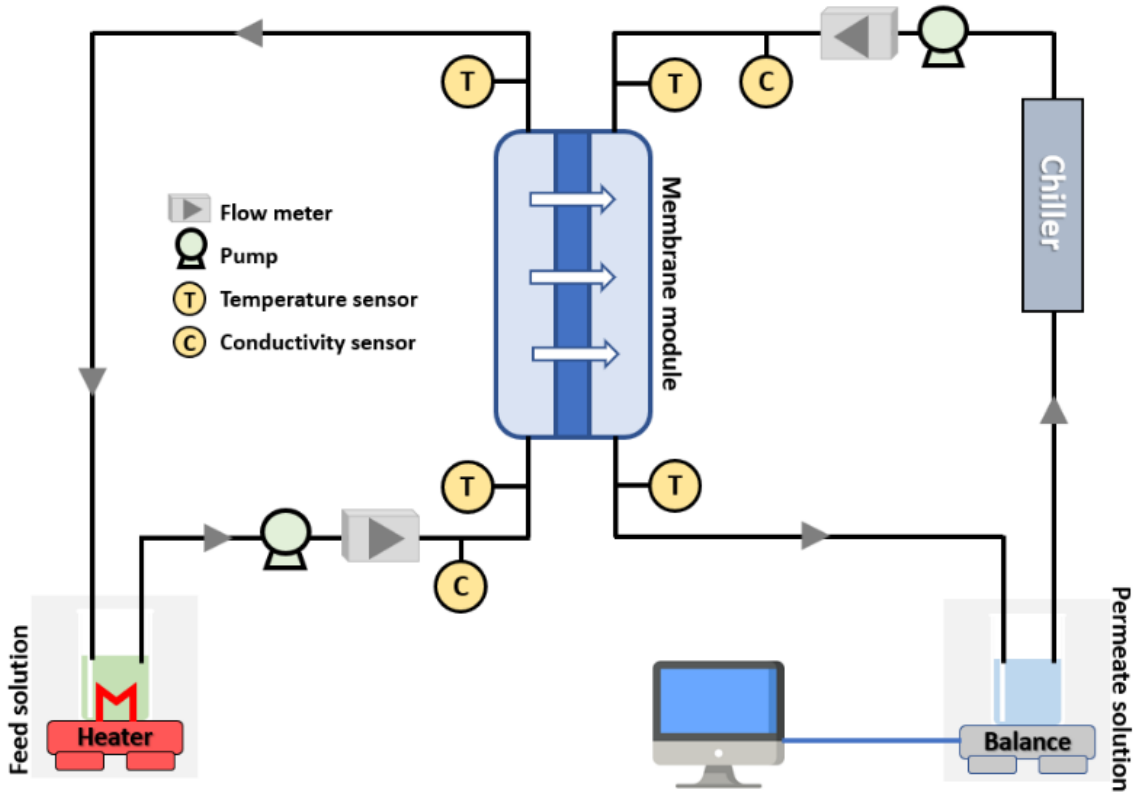

Fig.3 Schematic diagram of the DCMD system

$$J = \frac{\Delta m}{A\,\Delta t}$$

Where A is an effective area of the membrane (equal to 0.0478 m^2) and t is time in hour [36]. In addition, the conductivity was constantly measured to evaluate the salt rejection which was calculated by the following equation:

$$R = \left(1 - \frac{C_p\left(\frac{v_0}{v_p} + 1\right)}{C_f}\right) \times 100$$

Where C_p and C_f represent the solute concentration in both permeate and feed solutions (mol L^{-1}), respectively, v_0 and v_p represent the initial water volume and final water volume of permeate at a specific time [37].

1. Result and discussion

3.1. Dope solution characterizations

Hansen solubility parameters (HSP) are utilized to estimate the possibility of miscibility of two or more materials. Thus, The HSP can be written as:

$$R_{A-B} = \sqrt{(\delta_{dA} - \delta_{dB})^2 + \left(\delta_{pA} - \delta_{pB}\right)^2 + (\delta_{hA} - \delta_{hB})^2}$$

The Relative Energy Density (RED) gives the radius of interaction that describes the relative compatibility between two components, and it can be written as [26]:

$$RED = \frac{R_{A-B}}{R_0}$$

Indeed, all binary solvents' RED values were less than one, which confirms the ability of solvents to dissolve the polymer. As the production of the membranes in electrospinning depends on several factors, including the rate of solvent evaporation which is measured by the vapor pressure concept. Vapor pressure always indicates the volatility of the solvent and can be calculated according to Raoult's law by the following equation:

$$P = P_a X_a + P_b X_b$$

The purpose of utilizing binary solvents is to control the vapor pressure, which in turn controls the solvent's evaporation rate during the electrospinning process. Since acetone has a high vapor pressure (25 kPa), it is usually mixed with the major solvent to accelerate solvent evaporation and fabricate a dry membrane. The high vapor pressure of the binary solvents ensures the possibility of using dope solutions in electrospinning and producing a dry membrane. The vapor pressure of binary solvents (i.e., DMF/Acetone) is listed in Table **2**. which increased with increasing acetone weight fraction.

Table 2. Properties of solvent systems

Solvents systems	FA 6-4	FA 5-5	FA 4-6
Solubility parameter $(MPa)^{1/2}$	4.34	5.69	7.11
RED	0.45	0.59	0.74
vapor pressure (kPa)	11.59	14.08	16.46

The viscosity and surface tension of solutions are critical properties in the electrospinning process, so they should be in an appropriate range where the process cannot proceed under or above this range. At high viscosity, the polymer extrusion is impossible, while at low viscosity, the droplets of the polymer may interrupt. The surface tension usually determines the voltage used in electrospinning that is required to be overcome. They are determined by solvents ratios and polymer percentage [8]. As shown in Table **3**, in DMF/Acetone (FA 6-4 Px, x=6,8,10%) dope solutions, the viscosity increased with increasing polymer content to be 70, 175, and 405 cp, respectively, but it decreased with fixing polymer percentage and increasing the weight fraction of acetone. Overall, in this study, the suitable viscosity for electrospinning was found in a range between 70 to 400 cp for all DMF/Acetone dope solutions. Viscosity and surface tension values were found in the appropriate range for electrospinning that was reported in the literature [38,39].

Table 3. Properties of PVDF-HFP dope solutions.

Dope solutions	FA 6-4 P6	FA 6-4 P8	FA 6-4 P10	FA 5-5 P10	FA 4-6 P10
Viscosity (cp)	70	175	405	375	339.5
Surface Tension ($mN\ m^{-1}$)	38.5	39.52	37.82	37.24	35

3.2. Membrane surface characterizations

Concerning the structural properties of the membrane, the thickness, porosity, pore size, and contact angle were investigated to ensure that the membranes are suitable for water treatment applications. Table 4. shows the thickness and pore size results of PVDF-HFP nanofibers membranes. The polymer percentage used in the preparation of the nanofibers membranes affects the thickness of these membranes. For example, FA 6-4 P6 membrane has a thickness of 64.8 μm, which increased as the polymer percentage increased from 8% to 10%. FA 6-4 P6 and FA 6-4 P8 membranes have a thickness of 184 and 251 μm, respectively. Further, the difference in thickness of these three membranes was a little small between FA 6-4 P6 and FA 6-4 P8 membranes but was largely from FA 6-4 P10 membrane which may result from the difference in fiber collection time during electrospinning. The electrospinning of the FA 6-4 P10 membrane took longer time than the other two membranes. In the case of fixing the polymer percentage and increasing the acetone weight fraction, the membrane became thinner. The thickness of FA 5-5 P10 and FA 4-6 P10 membranes sharply decreased to 103 and 77.5 μm, respectively, compared with the FA 6-4 P10 membrane. In addition, the NIPS membrane was the thinnest one compared to all nanofibers membranes. In the same way, the increase in acetone weight fraction affected the mean pore size to become narrow. The FA 4-6 P10 membrane with the highest amount of acetone possesses a mean pore size that is smaller than the FA 5-5 P10 and FA 6-4 P10 membranes. The polymer percentage has little effect on the mean pore size, but all membranes, in this case, recorded the mean pore sizes in the same range between 202 and 218. However, the mean pore size of all prepared membranes was found in a good range, lower than 0.3 μm (300 nm). The results showed that the thickness of the membrane is directly proportional to the viscosity of the dope solution. So, with the increase in the viscosity of dope solutions, the thickness of the membranes increases and vice versa. In addition, especially when fixed polymer percentage, the thinner nanofibers

membrane tends to form a smaller pore size [40].

Table 4. Mean thickness and pore size results of PVDF-HFP electrospun nanofibers membrane.

Membrane	Mean Thickness (μm)	Mean pore size (nm)
FA 6-4 P6	64.8 ± 7.8	218 ± 5
FA 6-4 P8	184 ± 11.4	203 ± 5
FA 6-4 P10	251 ± 15.7	217 ± 5
FA 5-5 P10	103 ± 18.9	180 ± 5
FA 4-6 P10	77.5 ± 18.7	178 ± 5
FA 4-6 P10 NIPS	50.75 ± 4.2	-

The porosity of electrospun PVDF-HFP membranes was tested in Kerosene and the results are shown in Fig.4 Firstly, the porosity of nanofibers membranes increased as the PVDF-HFP percentage increased which was recorded the highest percent with FA 6-4 P10

membrane. The porosity of FA 6-4 P10 was 73.07% while the porosity of FA 6-4 P8 membrane and FA 6-4 P6 membrane were 68.46.16% and 60%, respectively. In the case of fixing polymer percentage, the porosities of three membranes (FA 6-4 P10, FA 5-5 P10, and FA 4-6 P10) were in the same range and did not largely affect by increasing acetone concentration. Unlike water uptake, the water uptake of the nanofibers membranes increases with the increase in acetone weight fraction. The lowest percent of water uptake was 33.3%, which was recorded by the FA 6-4 P10. The water uptake increased to 60 and 75% when the acetone weight fraction was increased in FA 5-5 P10 and FA 4-6 P10 membranes, respectively. Generally, all nanofibers membranes possess excellent porosity of greater than 60%.

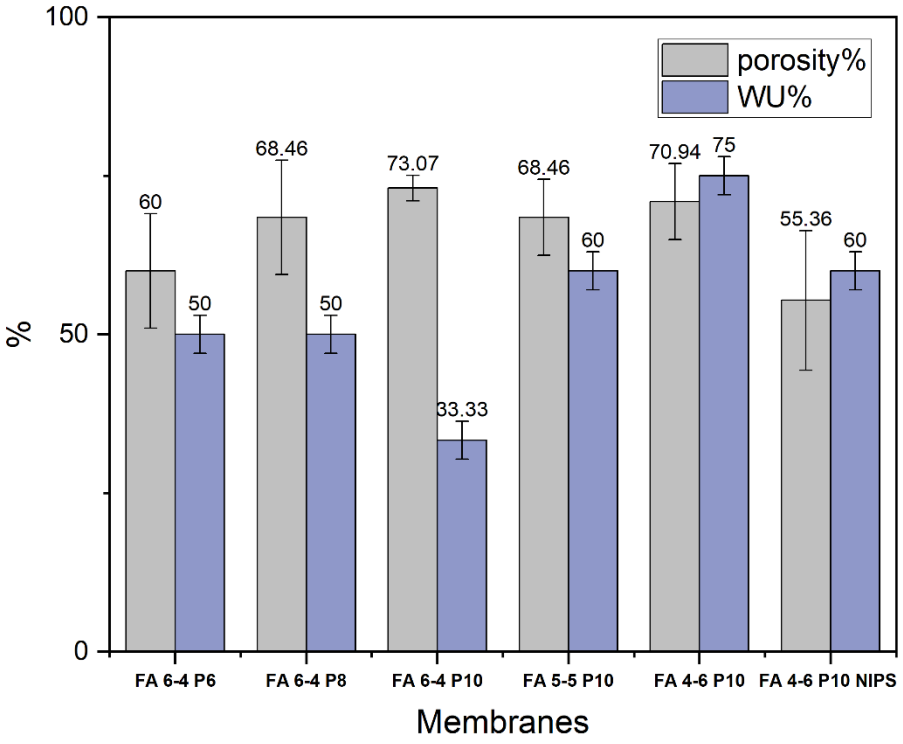

Fig.4 Porosities and WU of PVDF-HFP electrospun membranes

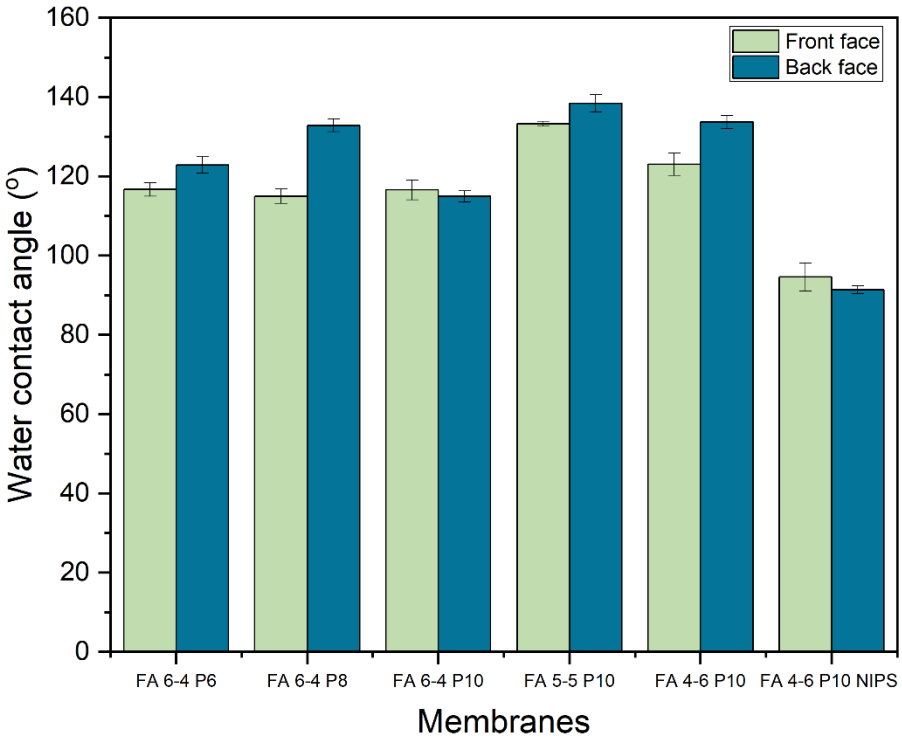

Fig.5 Water contact angles of PVDF-HFP electrospun membranes

The hydrophobicity of membranes was also tested by measuring the water contact angle for each face of the membrane. The results showed that almost the back face of all membranes has a higher hydrophobicity property. As shown in Fig.**5**, the highest contact angle was recorded by DMF/Acetone membranes in two ratios 5:5 and 4:6 (FA 5-5 P10 and FA 4-6 P10) on both sides which were 133.22°, 138.39°, and 122.98°, 133.66° for the front and back faces, respectively. Among membranes containing 10% of PVDF, the lowest contact angle was recorded by a weight ratio of 6:4 which was 116.56° for the front face and 114.95° for the back face. When the solvent weight ratio of DMF/Acetone was fixed at 6:4 with changed PVDF-HFP percent (FA 6-4 P6, FA 6-4 P8, and FA 6-4 P10), the back face of all membranes showed a superior water contact angle compared with the front face. According to the back face contact angle of DMF/Acetone membranes, the best percent of PVDF-HFP is 8% since its contact angle was 132.82°, whereas, in FA P6 and FA P10 membranes, it was 122.75° and 114.95° for the back face, respectively. On the other hand, the front faces of FA 6-4 P6 and FA 6-4 P10 membranes had almost the same contact angle of 116.65° and 116.56°, respectively. However, the front face contact angle of the FA 6-4 P8 membrane was significantly lower than the back face. Nonetheless, all membranes were sufficiently hydrophobic as their water contact angles were greater than 90° [41].

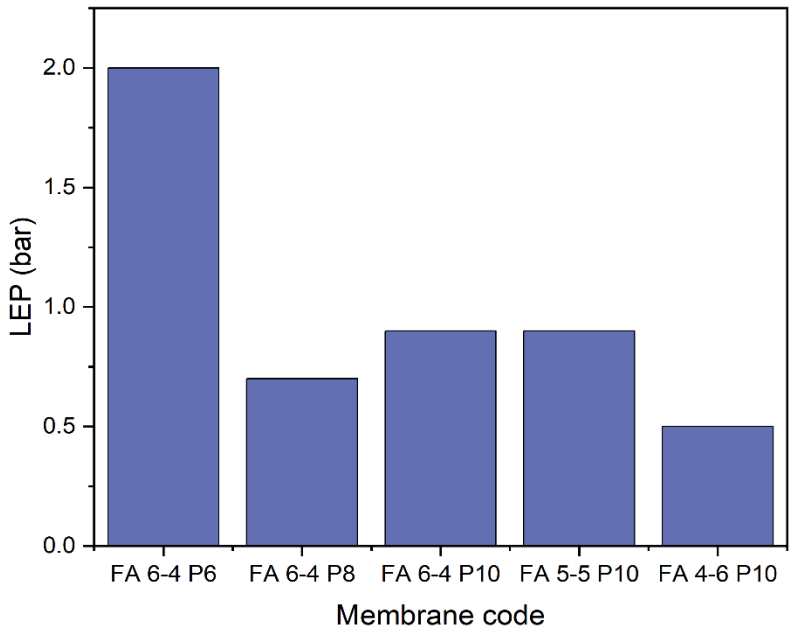

Fig.6 LEP values of PVDF-HFP electrospun

As shown in the literature, the LEP value of the membrane is directly influenced by the membrane thickness and pore size, and this explains the fluctuation of LEP values. The high LEP value refers to the low pore size and the optimum thickness of the membrane. Fig. 6 shows membrane LEP values. Membranes with different polymer weights (FA 6-4 P6, FA 6-4 P8, and FA 6-4 P10) showed the membrane with the lowest polymer percent (FA 6-4 P6) has the highest LEP, which resulted from its lower pore size. The LEP value increased from 0.7 to 0.9 bar with the polymer percentage increasing from 8% in FA 6-4 P8 membrane to 10% in FA 6-4 P10 membrane, as a result of a decrease in pore size and increased thickness. In the case of an equal weight fraction of DMF and acetone, the LEP value remained at 0.9 bar as for FA 6-4 P10 membrane, even though FA 6-4 P10 membrane has a much higher thickness compared to FA 5-5 P10 membrane, and this difference may have disappeared because FA 6-4 P10 membrane possessed a larger pore size than FA 5-5 P10 membrane, which accelerated wettability and reduced LEP value. In contrast, when the weight fraction of acetone was higher than that of DMF (FA 4-6 P10), the LEP value reduced to 0.5 bar since the thickness of the membrane significantly decreased but the pore size slightly decreased [42,43].

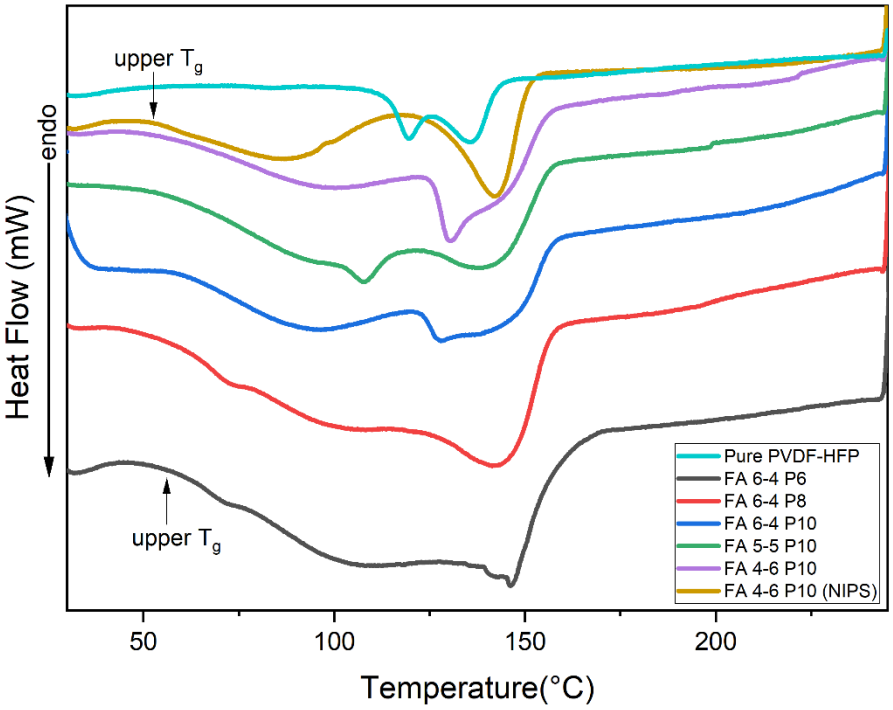

Fig.7 DSC results of PVDF-HFP electrospun nanofibers membranes

The crystalline phase composition and thermal properties of pure PVDF-HFP and nanofibers membranes were investigated by the DSC technique. The DSC thermograms of PVDF-HFP and nanofibers membranes are presented in Fig. **7**. It should be noted that the glass transition temperature (Tg) of PVDF-HFP is around -35 °C, as mentioned in the literature [44]. From the DSC curves, thermodynamic parameters were calculated and listed in Table **5**. As shown in Table. **5**, the increase in PVDF-HFP content leads to an increase in melting enthalpy and crystallinity percent, which was observed in three membranes of FA 6-4 Px (x= 6, 8, and 10). The FA6-4 P6 had a very low melting enthalpy and crystallinity percent compared to FA 6-4 P8 and FA 6-4 P10. The values of melting enthalpy and crystallinity of membranes containing 8 and 10% are very close. Thus, in membranes produced with a high polymer percentage, the crystalline region was higher than the amorphous region. Overall, the crystallinity of all nanofibers membranes was in the very low range and lower than the crystal content of pure PVDF-HFP.

Table 5. DSC results of pure PVDF-HFP and nanofibers membranes

Membranes	Pure PVDF-HFP	FA 6-4 P6	FA 6-4 P8	FA 6-4 P10	FA 5-5 P10	FA 4-6 P10	FA 4-6 P10 (NIPS)
T_m (^{0}C)	119.90 135.37	148.0	144.0	142.5	142.1	130.6	142.32
Upper T_g (^{0}C)	-	67.36	66.98	72.07	73.5	79.23	56.61
ΔH_m (J g^{-1})	12.10	3.954	9.705	8.62	12.35	11.48	10.76
X %	11.56	3.77	9.26	8.23	11.79	10.96 ±	10.27

The pure PVDF-HFP curve, as shown in Fig. 6, has two peaks; however, the nanofibers membrane curves have only one peak, with the other appearing as a broad low peak or broad drop in the curve line. An endothermic peak appeared between 130 and 148 ^{0}C in different nanofibers membranes due to PVDF-HFP copolymer melting. Some studies reported that the first curve that appeared in the range of 50 to 125 ^{0}C in different nanofibers membranes was considered a peak, and it refers to the presence of residual moisture [45,46]. The other suggested that the double peak of melting is attributed to its polymorphic structure; it was also referring to the presence of recrystallization of molten polymer and imperfect crystals in pure PVDF-HFP. Further, it may be related to the difference in the arrangement of bonding like "head-to-head" or "tail-to-tail" in PVDF-HFP membranes, which affects their thermodynamic behavior and crystalline phase formation [47,48]. Further research revealed that this curve is not considered an individual peak but rather a drop caused by phase transition [49]. Briefly, this peak was difficult to describe; therefore, it was also considered related to upper glass transition, reorganization inside α-crystals, melting of paracrystalline domains, or molecular motions corresponding to an α-relaxation in the crystalline/amorphous interface. Overall, the DSC result concluded that the amorphous phase dominates in all nanofibers membranes and the crystallinity is very low [50].

The FTIR results of different nanofibers are presented in Fig.8. FTIR peaks give information about the functional groups and crystalline phases that exist in membranes. Thus, the vibrational peak at 471 cm^{-1} is attributed to C–F wagging vibrations. The bands observed at 839 cm^{-1} and 795 cm^{-1} are assigned to CH_2 rocking vibrations, while its swinging vibration was shown at 1179 cm^{-1}. The vibrational peaks at 509 and 1279 cm^{-1} are assigned to the bending and asymmetric stretching vibrations of the CF_2 group. The peak observed at 1399 cm^{-1} is related to the wagging vibration of CH_2 or stretching vibrations of the CF group. All these vibrational peaks were found in the FTIR spectra of pure PVDF-HFP and all nanofibers membranes. Besides that, the crystallinity of pure PVDF-HFP and all nanofibers membranes was illustrated by FTIR and XRD peaks. The crystalline content of PVDF is less than 60%, as mentioned in the literature. Nonetheless, the amorphous part is not well studied and no trusted information about how it affects the XRD and FITR spectra is found. So, this part focused on describing the crystalline phases of pure PVDF-HFP and its nanofibers membranes. Peaks of FTIR and XRD spectra describe the non-polar crystalline (i.e. α-phase) and polar β and γ-phases. The non-polar crystalline α-phase of pure PVDF-HFP was observed at 1064, 795, 760, 612, 509, and 485 cm^{-1}, while the peaks at 1300, 1279, and 839 cm^{-1} assigned to amorphous β-phase and 1179 cm^{-1} for γ-phase. The dual character peaks that appeared at 975 were due to a mixture of α and γ-phases while 871 cm^{-1} was attributed to a mixture of β and γ-phases [23,51–53]. As shown in Fig.8, some peaks of non-polar crystalline α-phase disappeared in the spectra of membranes which exhibited in pure PVDF-HFP spectra, but still, the other peaks of α-phase appeared even though with lower intensity (i.e. 485, 509, 612 and 1064 cm^{-1}). Furthermore, all vibrational peaks of amorphous polar β-phase and semi-polar γ-phase appeared more intensely and broadly compared to the same peaks in pure PVDF-HPF spectra. However, these results reveal that all membranes contain amorphous polar β-phase and semi-polar γ-phase and a very slight amount of non-polar α-phase. Changing the solvent weight ratio in DMF/Acetone binary solvents could influence the volatility of the solvent system, consequently affecting the evaporation rate during electrospinning. The vapor pressure of each solvent system indicates the evaporation rate, which increased as the acetone weight ratio increased. In summary, as the volatility, vapor pressure, evaporation rate, or voltage are increased during electrospinning, so does the formation of the β-phase in the produced membrane [54,55].

 doi:10.20944/preprints202305.1577.v1

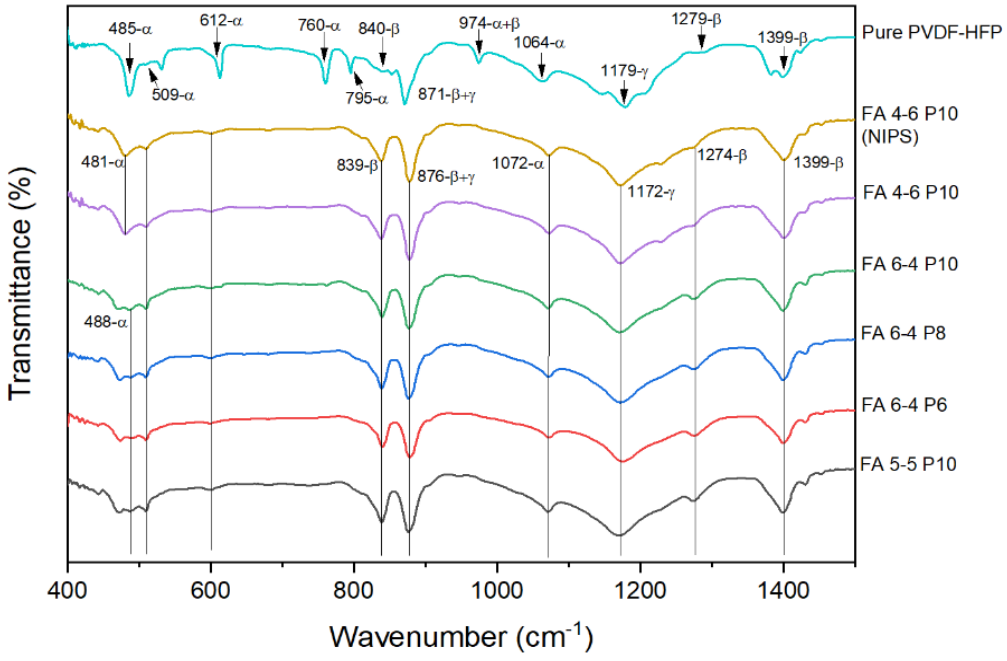

Fig.8 FTIR results of PVDF-HFP electrospun membranes

The XRD spectra of pure PVDF-HFP and nanofibers membranes provided good agreement with the FTIR results. Where XRD spectra revealed peaks corresponding to crystalline non-polar α-phase and amorphous polar β and γ-phases, as previously FTIR spectra had revealed. The XRD spectra of nanofibers membranes were presented in Fig. 8. The strong peaks at 17.6, 18.4, and 19.9 correspond to 100, 020, and 110, respectively, which are related to the non-polar α-phase. This finding demonstrates that the α-phase exists as the primary phase in powder PVDF-HFP. This does not mean that the PVDF-HFP contains only α-phase but also contains the γ and β-phase which appeared in weak peaks at 20.3 and 20.9, corresponding to 101 and 110/200, respectively. All PVDF-HFP electrospun nanofibers membranes show the peaks of α-phase and amorphous polar β and γ-phases. Finally, DSC and FTIR confirmed XRD results, all nanofibers membranes exhibited a semi-crystalline nature.

(a)

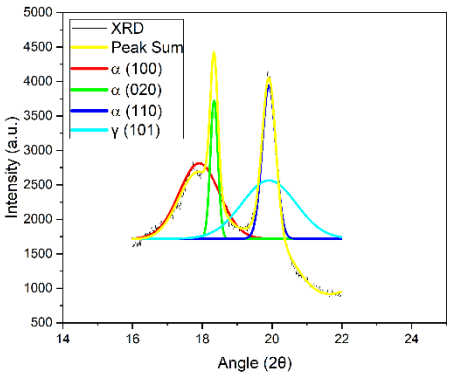

(b)

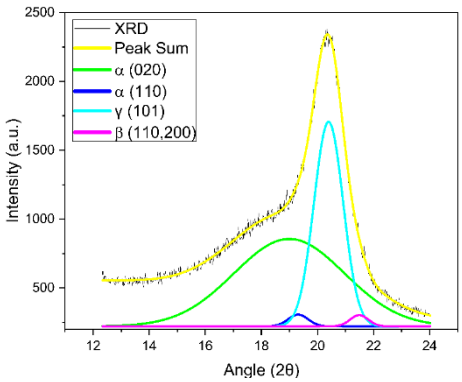

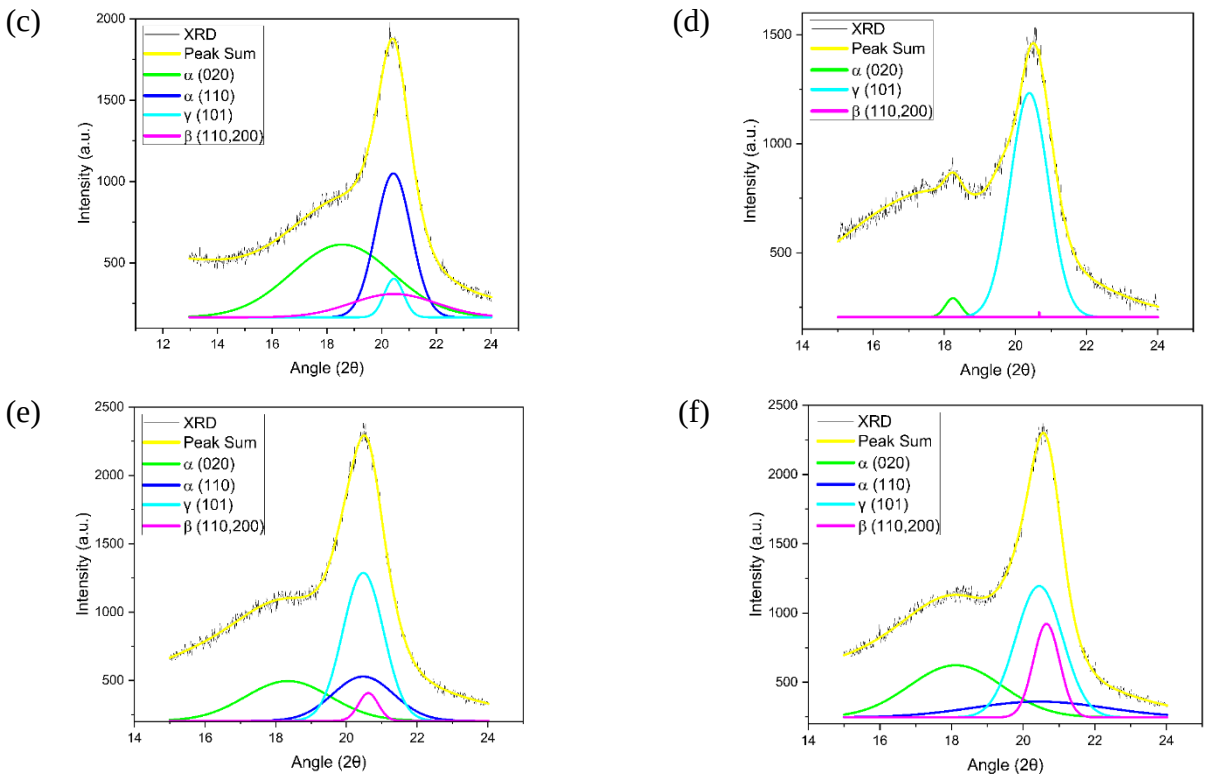

Fig.9 A typical deconvoluted XRD patterns for α, β, and γ-phases of (a) Pure PVDF-HFP (b) FA 6-4 P6; (c) FA 6-4 P8; (d) FA 6-4P10; (e) FA 5-5 P10; (f) FA 4-6 P10.

Morphological studies:

To evaluate the morphological structure of PVDF-HFP nanofibers membranes, the AFM technique was used. It was used to examine the internal construction of polymeric nanofibers and determine the average fiber diameter (AFD). From the 3D AFM images (Fig. 10), the average surface roughness (R_a) and root mean square roughness (R_q) were calculated for PVDF-HFP nanofibers membranes and listed in Table 6. AFM found that the average surface roughness of the nanofibers membranes increased with polymer percentage. The higher average surface roughness was recorded by the membrane produced by the highest weight ratio of acetone (FA 4-6 P10), which agreed with its contact angle (133.66 ^{0}). When the weight ratio of DMF and acetone was equal, the average surface roughness sharply decreased to 258.1 nm. In the same way, the root mean square roughness was 697.8 nm for the FA 6-4 P10 membrane, which was the highest value. Since FA 6-4 Px (x = 6 and 8) polymeric solution has a high surface tension of 38.5 and 39.52 mNm^{-1}, it forms a lot of beads in fibers. Because the surface tension of the polymeric solution in the FA 6-4 P10 membrane was lower, this effect vanished. Thus, the lower polymer concentration always increases the beads' formation and produces non-uniform fibers. This concluded that when surface tension is lower or equal to 37 mNm^{-1}, such as in the case of FA 6-4 P10, FA 5-5 P10, and FA 4-6 P10 polymeric solutions, smooth and uniform nanofibers will be produced. When the surface tension is above 37 mNm^{-1}, beads start to form on un-uniform fibers and nanofibers networks that are heterogeneous, as shown in Fig. 10 (a), (b), and (c). In addition, polymer concentration is an essential parameter that affects the way of spinning the polymeric solution in the electrospinning and, consequently, the morphology of fibers in electrospun membranes.

The AF 6-4 P6 membrane exhibits heterogeneous networks with un-uniform beaded nanofibers while the nanofibers got better in the 6-4 P8 membrane, where the fiber was more regular and the formation of the beads on the fibers was decreased. However, the nanofibers networks were almost organized (homogeneous), with smoother fibers in the membrane produced with a high polymer

percent of FA 6-4 P10 (high viscosity). Polymeric solutions with a high polymer percentage have a good viscoelastic force that makes the jet during electrospinning continuously elongates due to it fitting the coulombic and electrostatic forces. Whereas the jet of the polymeric solution with a low polymer percentage undergoes partial fracture because its viscoelastic force is low and can not fit the other forces that affect the electrospinning operation [29,38]. On the other hand, the beads did not form on the nanofibers of FA 5-5 P10 and FA 4-6 P10 membranes, as observed in Fig. 10 (d) and (e), and the nanofibers were perfectly entangled. The viscosities of polymeric solutions (375 and 339.5 cp for FA 5-5 P10 and FA 4-6 P10) are attributed to this effect because they are higher than the viscosities of AF 6-4 P6 and FA 6-4 P8, which have viscosities of 70 and 175 cp and do not have these features. The second thing that may be responsible for this behavior is the solvent evaporation rate during the electrospinning process which is influenced by the vapor pressure and volatility property of the solvent. DMF has a low vapor pressure and volatility whereas acetone has a high vapor pressure and volatility, therefore, different solvents mixing composition resulted in different volatility and vapor pressure. In addition, the smaller fiber diameter produced by the solution possesses low viscosity and low vapor pressure (high boiling point) [56]. The requirement for low viscosity is to produce fine fibers to prevent polymer macromolecules from becoming entangled as occurs on solutions with high viscosity [38]. In addition, the morphology of the NIPS membrane in Fig. 10 (f) differs from all other membranes (Fig. 10 from (a) to (e)). The NIPS membrane shows a spongy texture, while the electrospun membranes show nanofibers. The roughness of the NIPS membrane was sharply decreased to be at the lowest level compared to all electrospun nanofibers membranes, and the lowest difference in Ra values between them is 144 nm. These observations explain the previous contact angle results, which showed that the contact angle of the NIPS membrane was much lower than the contact angle of all electrospun nanofibers membranes.

Table 6. Roughness parameters for various PVDF-HFP nanofibers membranes

Membranes	R_a (nm)	R_q (nm)	AFD (µm)
FA 6-4 P6	284.1	367.83	1.20 ± 0.5
FA 6-4 P8	373.84	477.06	1.21 ± 0.2
FA 6-4 P10	382.06	455	1.78 ± 0.4
FA 5-5 P10	258.01	324.33	0.93 ± 0.5
FA 4-6 P10	593.83	697.8	1.67 ± 0.4
FA 4-6 P10 (NIPS)	114.39	136.46	-

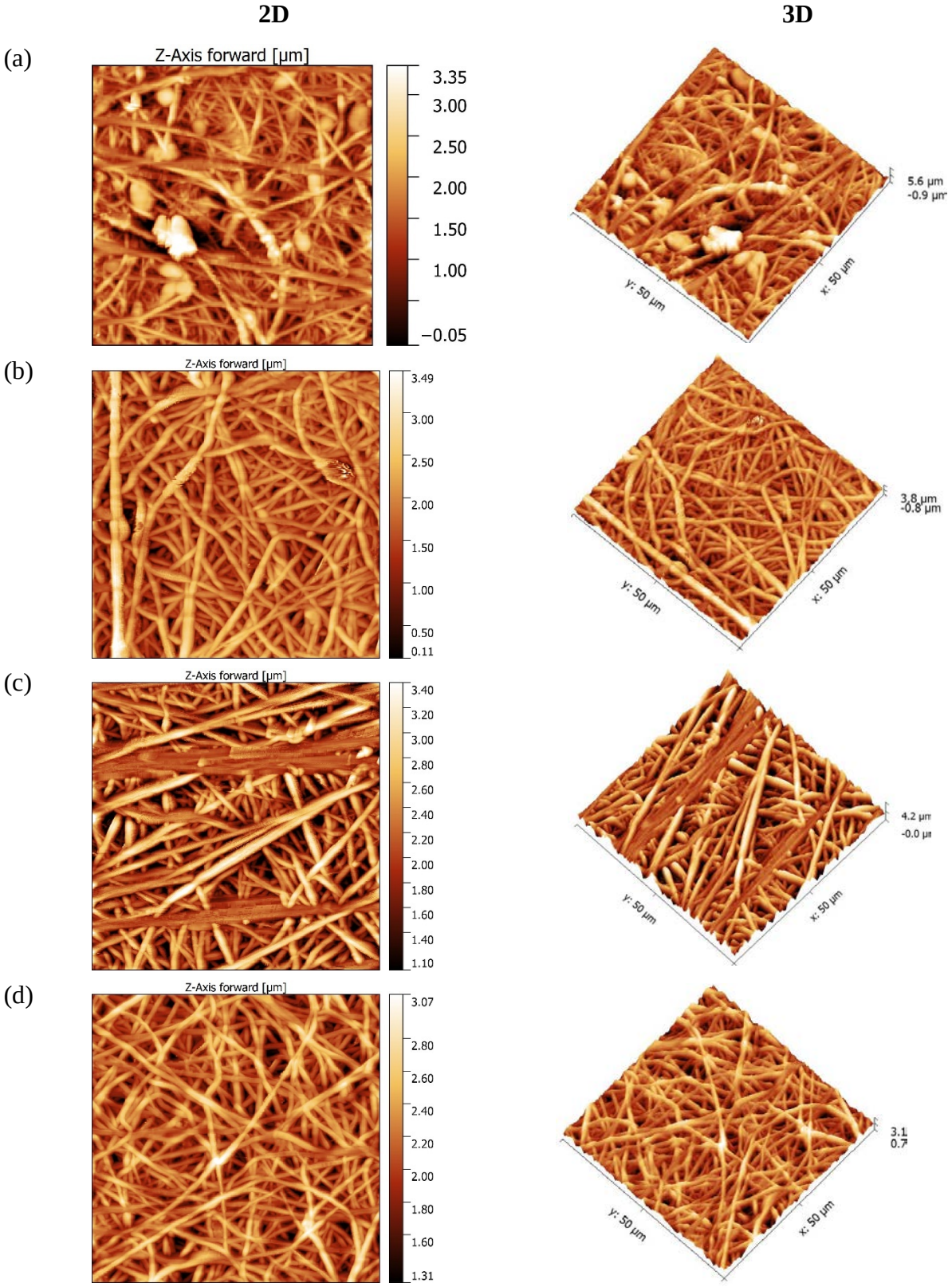

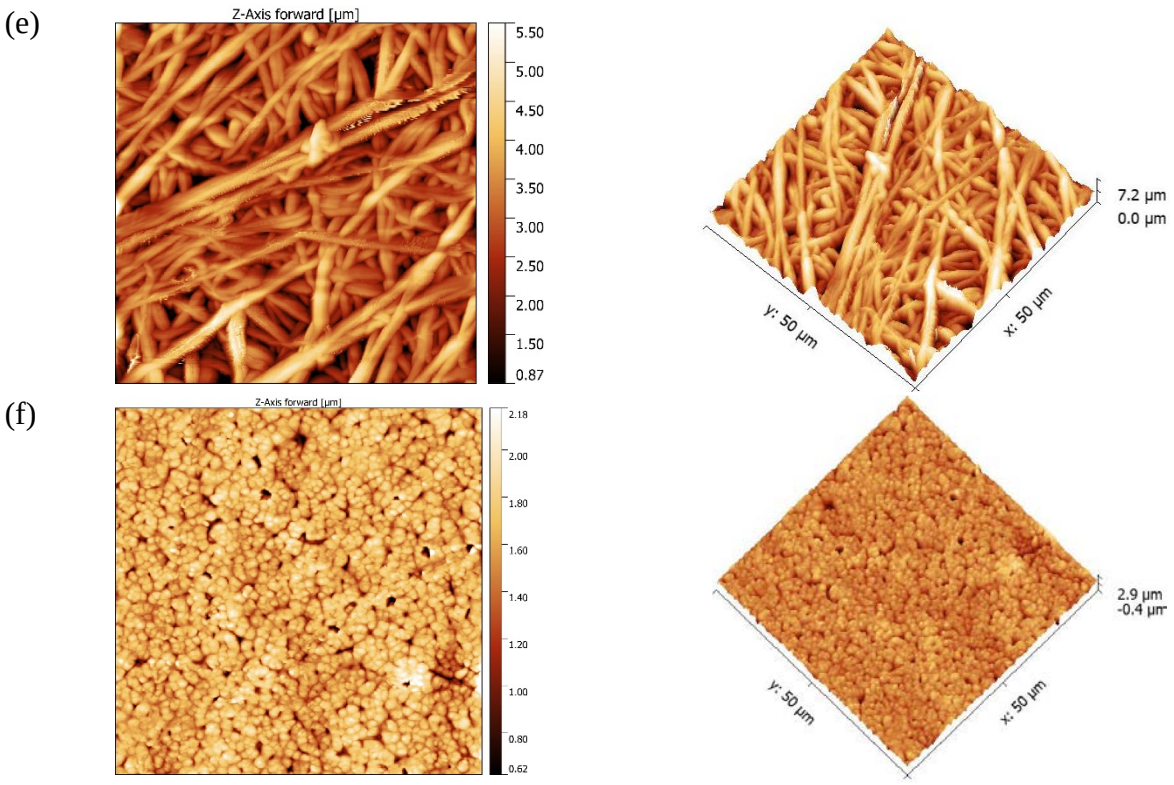

Fig.10 2D and 3D AMF images of (a) FA 6-4 P6; (b) FA 6-4 P8; (c) FA 6-4P10; (d) FA 5-5 P10; (e) FA 4-6 P10 and (f) FA 4-6 P10 (NIPS) membranes.

3.3. DCMD application

MD tests were used to evaluate the performance of different PVDF-HFP nanofibers membranes. The feed side used brine water at 70 ^{0}C, and the permeate temperature was 20 ^{0}C. Water vapor passed through the pores of the membranes due to the difference in vapor pressure between the two sides. The NIPS membrane did not give any flux of water under these experimental conditions because it has a very small pore size and very low porosity. Table 7. shows the average water flux and salt rejection of different nanofibers membranes. Since the FA 6-4 P6 membrane exhibits a larger pore size and higher porosity than FA 6-4 P8 and FA 6-4 P10 membranes, it also exhibits good permeability in the MD test. As can be seen in Fig.11, the flux of water was maintained above 25 kg m^{-2} h^{-1} during the two-hour test by three different membranes FA 6-4 P6, FA 5-5 P10, and FA 4-6 P10. They achieved a higher water flux compared to the PVDF membrane filter disc. According to the average water flux listed in Table 7, the PVDF membrane filter disc provided 22 kg m^{-2} h^{-1}, while FA 6-4 P6, FA 5-5 P10, and FA 4-6 P10 were all greater than 38 kg m^{-2} h^{-1}. The other two membranes, FA 6-4 P8, and FA 6-4 P10, gave very close average water flux values to that of PVDF membrane filter disc and showed almost the same behavior. The behavior of FA 6-4 Px (x = 6, 8, and 10) membranes in the MD test shows that as the PVDF-HFP content increased, the water flux decreased. This result is expected due to the hydrophobicity property of PVDF-HFP, which increased as the polymer content rose. The roughness of membranes also increased as the polymer content increased, which made the membranes have high hydrophobicity and made it difficult for vaporized water to pass across the membrane pores. Since the porosity is directly proportional to the permeability of the membrane, this provided a good argument for these results. As mentioned previously, the porosities of the FA 6-4 Px (x = 6, 8, and 10) membranes were 81.27, 79.16, and 63.45%, respectively, consequently, the permeability was found to be higher in the FA 6-4 P6 membrane than in the FA 6-4 P8 membrane and at a lower level in the FA 6-4 P10 membrane. The permeability behavior of FA 6-4 Px (x = 6, 8, and 10) membranes in the first 50 min was constant; after that, it slightly decreased, except for FA 6-4 P10 membrane. On the other hand, even though the porosity of FA 6-4 P10 membrane was higher than the porosities of FA 5-5 P10 and FA 4-6 P10 membranes by 5%, the permeability of FA 5-5 P10 and FA 4-6 P10 membranes had increased by approximately 20 kg m^{-2} h^{-1} compared the permeability of FA 6-4 P10 membrane.

The average salt rejection of PVDF-HFP nanofibers membranes was found above 90% as shown in Table 7, which proves the efficiency of these nanofibers membranes in water treatment and contamination removal. The FA 5-5-P10 membrane achieved perfect performance in terms of permeability and salt rejection. Even though the lower water flux in the MD test was achieved with FA 6-4 P8 and FA 6-4 P10 membranes, they achieved a higher salt rejection percent (99.9%). FA 6-4 P6 and FA 4-6 P10 membranes have a high water flux but slightly lower salt rejection (91.5% and 91.7%, respectively) compared to others. Regardless, during MD experiments, all PVDF-HFP electrospun nanofibers membranes demonstrated good permeability and salt rejection for two hours with no damaged or sharply increased conductivity.

(a)

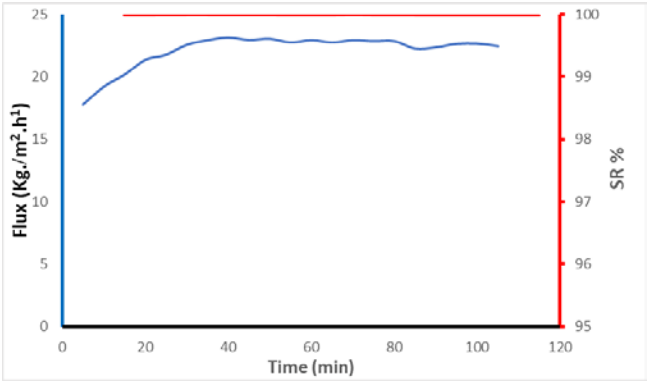

(b)

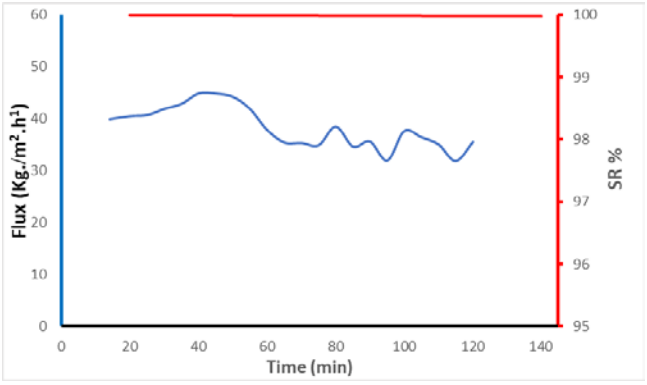

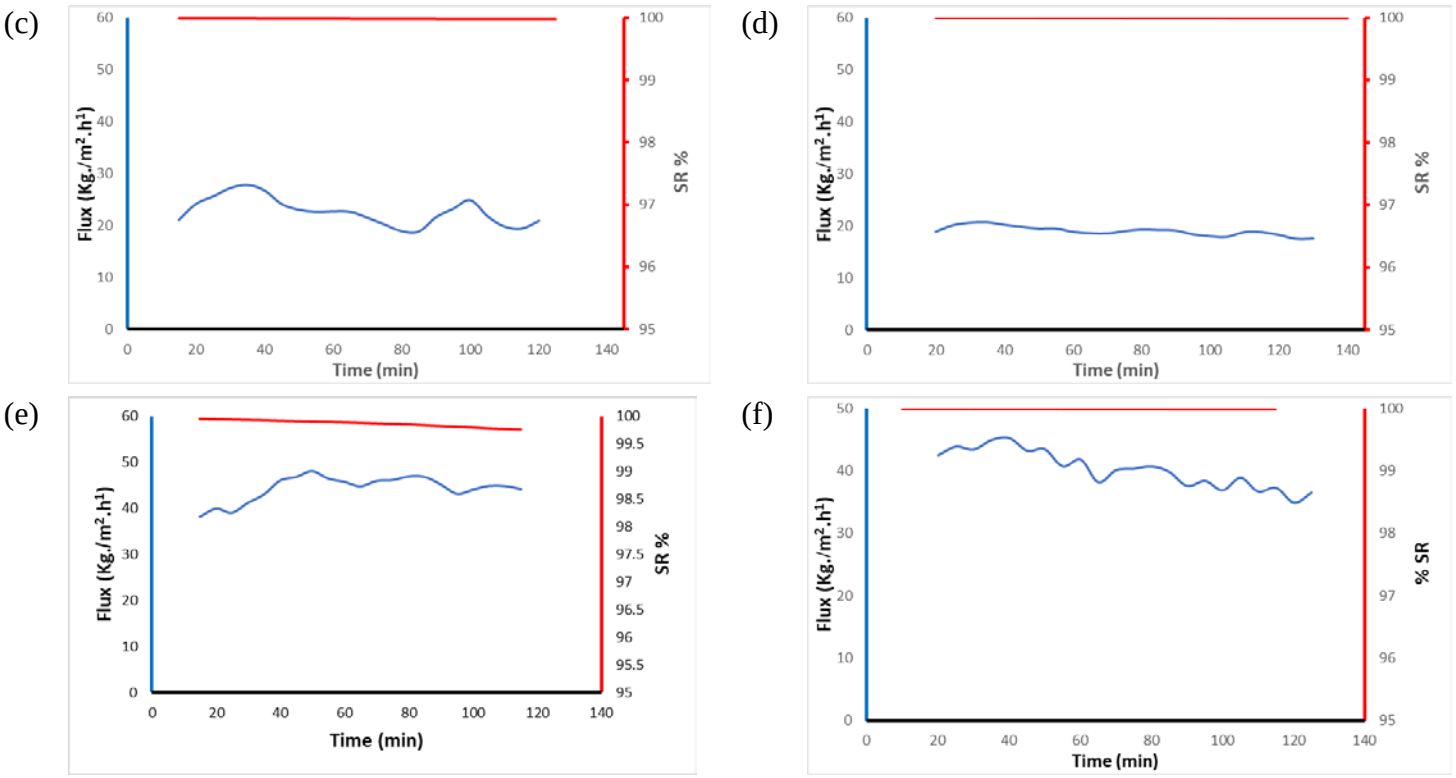

Fig.11 DCMD water flux (blue line) and salt rejection (red line) vs time plot for (a) PVDF (b) FA 6-4 P6; (c) FA 6-4 P8; (d) FA 6-4P10; (e) FA 5-5 P10; and (f) FA 4-6 P10

Table 9. Average water flux and salt rejection of all nanofibers membranes during the MD test

Membrane code	Average water flux (kg m^{-2} h^{-1})	Average salt rejection (%)
PVDF membrane filter disc	22.1 ± 1.4	99.9
FA 6-4 P6	38.3 ± 4.0	91.5
FA 6-4 P8	22.7 ± 2.6	99.9
FA 6-4 P10	19.1 ± 0.9	99.9
FA 5-5 P10	44.4 ± 2.9	99.8
FA 4-6 P10	40.3 ± 2.9	91.7

4. Conclusion

In this work, PVDF-HFP nanofibers membranes were prepared with different solvent ratios and different polymer percentages through electrospinning. The preliminary tests for binary solvent compositions indicated that these compositions could be used in electrospinning to produce nanofibers membranes. A series of characterization tests were used to examine the ability to utilize these membranes in water treatment and predict their behavior during DCMD. The permeability of membranes was tested in terms of pore size and porosity, which concluded that the mean pore size

decreased as the weight ratio of acetone increased and the percentage of polymer used did not affect it greatly. In contrast, the polymer percentage has positively affected porosity. Pore size and thickness have a direct influence on LEP value which gives information about the wettability of the membranes. LEP values were found in a range between 2 and 0.5 bar. The hydrophobicity of nanofibers membranes was also tested through contact angle, which revealed that all PVDF-HFP nanofibers membranes possess a hydrophobic surface since their water contact angle is above 90 (between 114 and 33). DSC thermogram curves of PVDF- HFP nanofibers membranes showed a different behavior than pure PVDF-HFP. Two thermal peaks appeared in the curve of pure PVDF-HFP, but in the curves of nanofibers membranes, one thermal peak appeared between 130 and 148 0C with a broad curve in the range between 50 and 125 0C, which was difficult to explain. Some studies have classified this broad curve as an upper glass transition, reorganization within α-crystals, melting of paracrystalline domains, or molecular motions corresponding to α-relaxation at the crystalline/amorphous interface. Until now, the crystallinity of the co-polymer PVDF-HFP has been unclear, and efforts should be directed toward describing the broad thermal curve in DSC curves, as well as classifying DSC peaks according to phase (polar α-phase and amorphous polar β and γ-phases).

DSC, FTIR, and XRD results confirmed that all nanofibers membranes are semi-crystalline with polar α-phase and amorphous polar β and γ-phases. The NIPS membrane showed poor characteristics compared to electrospun nanofibers membranes, where its porosity, thickness, and water contact angle were much lower than those of nanofibers membranes. Because the NIPS membrane has a very low porosity, its LEP cannot be calculated and cannot be applied in DCMD. In DCMD, almost all membranes provided good results. Although the water flux was lower with FA 6-4 P8 and FA 6-4 P10 membranes, the salt rejection was very good. The perfect performance was found by FA 5-5 P10, which recorded the highest average water flux (44 kg m-2 h-1) and the highest salt rejection (99.8%). The water flux was found to be over 38 kg m-2 h-1 in three different membranes, FA 6-4 P6, FA 5-5 P10, and FA 4-6 P10, but it was constant throughout the experiment only with the FA 5-5 P10 membrane. Thus, among these membranes, the salt rejection was 99% only with FA 5-5 P10, while the others gave ~91.5%. The efficiency of PVDF-HFP nanofibers membranes for water treatment purposes was studied with brine water, but it can be tested with other types of wastewater.

This study recommends that the good membranes discovered be long-term tested and improved in performance by enhancing their hydrophobic properties via the insertion of nanoparticles on their surfaces.

Funding: This research was funded by the Deputyship for Research and Innovation, Ministry of Education in Saudi Arabia.

Acknowledgments: The authors extend their appreciation to the Deputyship for Research and Innovation, Ministry of Education in Saudi Arabia for funding this research work through the project number (751).

Conflicts of Interest: The authors declare no conflict of interest.

Reference

1. Ravi J, Othman MHD, Matsuura T, Ro'il Bilad M, El-badawy TH, Aziz F, et al. Polymeric membranes for desalination using membrane distillation: A review. Desalination 2020;490. https://doi.org/10.1016/j.desal.2020.114530.
2. Cui J, Li F, Wang Y, Zhang Q, Ma W, Huang C. Separation and Purification Technology Electrospun nanofiber membranes for wastewater treatment applications. Sep Purif Technol 2020;250:117116.
3. Liu Q, Chen Z, Pei X, Guo C, Teng K, Hu Y, et al. Review: applications, effects and the prospects for electrospun nanofibrous mats in membrane separation. J Mater Sci 2020;55:893–924. https://doi.org/10.1007/s10853-019-04012-7.
4. Jain H, Garg MC. Fabrication of polymeric nanocomposite forward osmosis membranes for water desalination—A review. Environ Technol Innov 2021;23. https://doi.org/10.1016/j.eti.2021.101561.
5. Kugarajah V, Ojha AK, Ranjan S, Dasgupta N, Ganesapillai M, Dharmalingam S, et al. Future applications of electrospun nanofibers in pressure driven water treatment: A brief review and research update. J Environ Chem Eng 2021;9:105107. https://doi.org/10.1016/j.jece.2021.105107.
6. Francis L, Ahmed FE, Hilal N. Advances in Membrane Distillation Module Configurations. Membranes (Basel) 2022;12. https://doi.org/10.3390/membranes12010081.

7. Chae SH, Kim JH. Integration of PRO into Desalination Processes. 2017. https://doi.org/10.1016/B978-0-12-812103-0.00004-0.
8. Liao Y, Loh C, Tian M, Wang R, Fane AG. Progress in Polymer Science Progress in electrospun polymeric nanofibrous membranes for water treatment : Fabrication , modification and applications. Prog Polym Sci J 2018;77:69–94.
9. Ismail MS, Mohamed AM, Poggio D, Pourkashanian M. Direct contact membrane distillation: A sensitivity analysis and an outlook on membrane effective thermal conductivity. J Memb Sci 2021;624:119035. https://doi.org/10.1016/j.memsci.2020.119035.
10. Chen M, Ding W, Zhou M, Zhang H, Ge C, Cui Z, et al. Fouling mechanism of PVDF ultrafiltration membrane for secondary effluent treatment from paper mills. Chem Eng Res Des 2021;167:37–45. https://doi.org/10.1016/j.cherd.2020.12.021.
11. Duong HC, Ansari AJ, Hailemariam RH, Woo YC, Pham TM, Ngo LT, et al. Membrane Distillation for Strategic Water Treatment Applications: Opportunities, Challenges, and Current Status. Curr Pollut Reports 2020;6:173–87. https://doi.org/10.1007/s40726-020-00150-8.
12. Liao Y, Wang R, Tian M, Qiu C, Fane AG. Fabrication of polyvinylidene fluoride (PVDF) nanofibers membranes by electro-spinning for direct contact membrane distillation. J Memb Sci 2013;425–426:30–9. https://doi.org/10.1016/j.memsci.2012.09.023.
13. Liang Y, Zhao J, Huang Q, Hu P, Xiao C. PVDF fiber membrane with ordered porous structure via 3D printing near field electrospinning. J Memb Sci 2021;618. https://doi.org/10.1016/j.memsci.2020.118709.
14. Jiang S, Ladewig BP. Green synthesis of polymeric membranes: Recent advances and future prospects. Curr Opin Green Sustain Chem 2020;21:1–8. https://doi.org/10.1016/j.cogsc.2019.07.002.
15. Huo P, Zhong CT, Xiong XP. Tailoring Morphology of PVDF-HFP Membrane via One-step Reactive Vapor Induced Phase Separation for Efficient Oil-Water Separation. Chinese J Polym Sci (English Ed 2021;39:610–9. https://doi.org/10.1007/s10118-021-2527-x.
16. Liu Z, Cao R, Wei A, Zhao J, He J. Superflexible/superhydrophilic PVDF-HFP/CuO-nanosheet nanofibrous membrane for efficient microfiltration. Appl Nanosci 2019;9:1991–2000. https://doi.org/10.1007/s13204-019-01014-4.
17. Das S, Ghosh A. Structure, ion transport, and relaxation dynamics of polyethylene oxide/poly (vinylidene fluoride co-hexafluoropropylene) - Lithium bis(trifluoromethane sulfonyl) imide blend polymer electrolyte embedded with ionic liquid. J Appl Phys 2016;119. https://doi.org/10.1063/1.4942658.
18. Liang Y, Cheng S, Zhao J, Zhang C, Sun S, Zhou N, et al. Heat treatment of electrospun Polyvinylidene fluoride fibrous membrane separators for rechargeable lithium-ion batteries. J Power Sources 2013;240:204–11. https://doi.org/10.1016/j.jpowsour.2013.04.019.
19. Gebreyesus MA, Purushotham Y, Kumar JS. Preparation and characterization of lithium ion conducting polymer electrolytes based on a blend of poly(vinylidene fluoride-co-hexafluoropropylene) and poly(methyl methacrylate). Heliyon 2016;2. https://doi.org/10.1016/j.heliyon.2016.e00134.
20. Fen W, Zhang H. Recent advances in polymer blend membranes for gas separation and pervaporation. Prog Mater Sci J 2021;116.
21. Saxena P, Shukla P. A comprehensive review on fundamental properties and applications of poly (vinylidene fluoride) (PVDF). Adv Compos Hybrid Mater 2021;4:8–26. https://doi.org/10.1007/s42114-021-00217-0.
22. Kalimuldina G, Turdakyn N, Abay I, Medeubayev A, Nurpeissova A, Adair D, et al. A Review of Piezoelectric PVDF Film by Electrospinning and Its Applications. Sensors 2020;20. https://doi.org/10.1088/2043-6262/1/4/043002.
23. Oumghar K, Chakhchaoui N, Farhane R, Eddiai A, Meddad M, Cherkaoui O, et al. Enhanced piezoelectric properties of PVdF-HFP/PZT nanocomposite for energy harvesting application. IOP Conf Ser Mater Sci Eng 2020;827:6–11. https://doi.org/10.1088/1757-899X/827/1/012034.
24. Polat K. Energy harvesting from a thin polymeric film based on PVDF-HFP and PMMA blend. Appl Phys A Mater Sci Process 2020;126:1–8. https://doi.org/10.1007/s00339-020-03698-w.
25. Martina P, Gayathri R, Pugalenthi MR, Cao G, Liu C, Prabhu MR. Nanosulfonated silica incorporated SPEEK/SPVdF-HFP polymer blend membrane for PEM fuel cell application. Ionics (Kiel) 2020;26:3447–58. https://doi.org/10.1007/s11581-020-03478-9.
26. Russo F, Ursino C, Sayinli B, Koyuncu I, Galiano F, Figoli A. Advancements in Sustainable PVDF Copolymer Membrane Preparation Using Rhodiasolv® PolarClean As an Alternative Eco-Friendly Solvent. Clean Technol 2021;3:761–86. https://doi.org/10.3390/cleantechnol3040045.
27. Sarkar S, Chakraborty S. Nanocomposite polymeric membrane a new trend of water and wastewater treatment: A short review. Ground Sustain Dev 2021;12. https://doi.org/10.1016/j.gsd.2020.100533.

28. Saleem H, Trabzon L, Kilic A, Zaidi SJ. Recent advances in nanofibrous membranes: Production and applications in water treatment and desalination. Desalination 2020;478. https://doi.org/10.1016/j.desal.2019.114178.
29. Tabe S. A review of electrospun nanofiber membranes. J Membr Sci Res 2017;3:228–39. https://doi.org/10.22079/jmsr.2017.56718.1124.
30. Su CI, Shih JH, Huang MS, Wang CM, Shih WC, Liu Y sheng. A study of hydrophobic electrospun membrane applied in seawater desalination by membrane distillation. Fibers Polym 2012;13:698–702. https://doi.org/10.1007/s12221-012-0698-3.
31. Liao Y, Wang R, Fane AG. Engineering superhydrophobic surface on poly(vinylidene fluoride) nanofibers membranes for direct contact membrane distillation. J Memb Sci 2013;440:77–87. https://doi.org/10.1016/j.memsci.2013.04.006.
32. Wu X, Wu X, Wang T, Zhao L, Bach Y. Omniphobic surface modification of electrospun nanofibers membrane via vapor deposition for enhanced anti-wetting property in membrane distillation. J Membr Sci J 2020;606.
33. Beyraghi F, Mirfarsi SH, Rowshanzamir S, Karimi A, Parnian MJ. Optimal thermal treatment conditions for durability improvement of highly sulfonated poly(ether ether ketone) membrane for polymer electrolyte fuel cell applications. Int J Hydrogen Energy 2020;45:13441–58. https://doi.org/10.1016/j.ijhydene.2020.03.022.
34. Samadianfard R, Seifzadeh D, Habibi-Yangjeh A. Sol-gel coating filled with SDS-stabilized fullerene nanoparticles for active corrosion protection of the magnesium alloy. Surf Coatings Technol 2021;419:127292. https://doi.org/10.1016/j.surfcoat.2021.127292.
35. Rahimpour A, Jahanshahi M, Mollahosseini A, Rajaeian B. Structural and performance properties of UV-assisted TiO 2 deposited nano-composite PVDF/SPES membranes. Desalination 2012;285:31–8. https://doi.org/10.1016/j.desal.2011.09.026.
36. Nthunya LN, Gutierrez L, Lapeire L, Verbeken K, Zaouri N, Nxumalo EN, et al. Fouling-resistant PVDF nanofibre membranes for the desalination of brackish water in membrane distillation. Sep Purif Technol 2019;228. https://doi.org/10.1016/j.seppur.2019.115793.
37. Rezaei M, Samhaber W. Wetting behaviour of superhydrophobic membranes coated with nanoparticles in membrane distillation. Chem Eng Trans 2016;47:373–8. https://doi.org/10.3303/CET1647063.
38. Russo F, Ursino C, Avruscio E, Desiderio G, Perrone A, Santoro S, et al. Innovative poly (Vinylidene fluoride) (PVDF) electrospun nanofibers membrane preparation using DMSO as a low toxicity solvent. Membranes (Basel) 2020;10:1–17. https://doi.org/10.3390/membranes10030036.
39. Nuamcharoen P, Kobayashi T, Potiyaraj P. Influence of volatile solvents and mixing ratios of binary solvent systems on morphology and performance of electrospun poly(vinylidene fluoride) nanofibers. Polym Int 2021;70:1465–77. https://doi.org/10.1002/pi.6218.
40. Bahrami M, Karimi-Sabet J, Hatamnejad A, Dastbaz A, Moosavian MA. Optimization and modification of PVDF dual-layer hollow fiber membrane for direct contact membrane distillation; application of response surface methodology and morphology study. Korean J Chem Eng 2018;35:2241–55. https://doi.org/10.1007/s11814-018-0038-4.
41. Serhan M, Sprowls M, Jackemeyer D, Long M, Perez ID, Maret W, et al. Total iron measurement in human serum with a smartphone. AIChE Annu Meet Conf Proc 2019;2019-Novem. https://doi.org/10.1039/x0xx00000x.
42. Hu X, Chen X, Giagnorio M, Wu C, Luo Y, Hélix-Nielsen C, et al. Beaded electrospun polyvinylidene fluoride (PVDF) membranes for membrane distillation (MD). J Memb Sci 2022;661. https://doi.org/10.1016/j.memsci.2022.120850.
43. Zheng R, Chen Y, Wang J, Song J, Li X-M, He T. Preparation of omniphobic PVDF membrane with hierarchical structure for treating saline oily wastewater using direct contact membrane distillation. J Memb Sci 2018;555:197–205. https://doi.org/10.1016/j.memsci.2018.03.041.
44. Shalu, Singh VK, Singh RK. Development of ion conducting polymer gel electrolyte membranes based on polymer PVdF-HFP, BMIMTFSI ionic liquid and the Li-salt with improved electrical, thermal and structural properties. J Mater Chem C 2015;3:7305–18. https://doi.org/10.1039/c5tc00940e.
45. Gradišar Centa U, Mihelčič M, Bobnar V, Remškar M, Slemenik Perše L. The Effect of PVP on Thermal, Mechanical, and Dielectric Properties in PVDF-HFP/PVP Thin Film. Coatings 2022;12. https://doi.org/10.3390/coatings12091241.
46. Yadav PS, Kumar V, Singh UP, Bhat HR, Mazumder B. Physicochemical characterization and in vitro dissolution studies of solid dispersions of ketoprofen with PVP K30 and d-mannitol. Saudi Pharm J 2013;21:77–84. https://doi.org/10.1016/j.jsps.2011.12.007.
47. Atanassov A, Kostov G, Kiryakova D, Borisova-Koleva L. Properties of clay nanocomposites based on poly(vinylidene fluoride-co- Hexafluoropropylene). J Thermoplast Compos Mater 2014;27:126–41. https://doi.org/10.1177/0892705712443249.

48. Dillon DR, Tenneti KK, Li CY, Ko FK, Sics I, Hsiao BS. On the structure and morphology of polyvinylidene fluoride-nanoclay nanocomposites. Polymer (Guildf) 2006;47:1678–88. https://doi.org/10.1016/j.polymer.2006.01.015.
49. Malmonge LF, Malmonge JA, Sakamoto WK. Study of pyroelectric activity of PZT/PVDF-HFP composite. Mater Res 2003;6:469–73. https://doi.org/10.1590/s1516-14392003000400007.
50. Merlini C, Barra GMO, Medeiros Araujo T, Pegoretti A. Electrically pressure sensitive poly(vinylidene fluoride)/polypyrrole electrospun mats. RSC Adv 2014;4:15749–58. https://doi.org/10.1039/c4ra01058b.
51. Chakhchaoui N, Farhan R, Eddiai A, Meddad M, Cherkaoui O, Mazroui M, et al. Improvement of the electroactive b-phase nucleation and piezoelectric properties of PVDF-HFP thin films influenced by TiO2 nanoparticles. Mater Today Proc 2019;39:1148–52. https://doi.org/10.1016/j.matpr.2020.05.407.
52. Yadav A, Singh K, Panda AB, Labhasetwar PK, Shahi VK. Membrane distillation crystallization for simultaneous recovery of water and salt from tannery industry wastewater using TiO2 modified poly(vinylidene fluoride-co-hexafluoropropylene) nanocomposite membranes. J Water Process Eng 2021;44. https://doi.org/10.1016/j.jwpe.2021.102393.
53. Shanthi PM, Hanumantha PJ, Albuquerque T, Gattu B, Kumta PN. Novel Composite Polymer Electrolytes of PVdF-HFP Derived by Electrospinning with Enhanced Li-Ion Conductivities for Rechargeable Lithium-Sulfur Batteries. ACS Appl Energy Mater 2018;1:483–94. https://doi.org/10.1021/acsaem.7b00094.
54. He Z, Rault F, Lewandowski M, Mohsenzadeh E, Salaün F. Electrospun PVDF nanofibers for piezoelectric applications: A review of the influence of electrospinning parameters on the β phase and crystallinity enhancement. Polymers (Basel) 2021;13:1–23. https://doi.org/10.3390/polym13020174.
55. Szewczyk PK, Gradys A, Kim SK, Persano L, Marzec M, Kryshtal A, et al. Enhanced Piezoelectricity of Electrospun Polyvinylidene Fluoride Fibers for Energy Harvesting. ACS Appl Mater Interfaces 2020;12:13575–83. https://doi.org/10.1021/acsami.0c02578.
56. Abbas D, Mu'min MS, Bonanno M, Thiele S, Böhm T. Active solution heating and cooling in electrospinning enabling spinnability from various solvents. J Appl Polym Sci 2022;139:1–11. https://doi.org/10.1002/app.52730.
57. [55] Ndlwana, L.; Sikhwivhilu, K.; Moutloali, R.; Ngila, J.C. Heterogeneous Functionalization of Polyethersulfone: A New Approach for pH-Responsive Microfiltration Membranes with Enhanced Antifouling Properties. J. Membr. Sci. Res. 2020, 6, 178-187.